Ultra-Compact Mode (De)Multiplexer and Polarization Beam Splitter Based on Tapered Bent Asymmetric Directional Couplers

JunBo Zhu, HaiYang Huang, YingXuan Zhao, Yang Li, XiaoJuan She, Han Liao, Rui Huang, ZiJian Zhu, Xiang Liu, Zhen Sheng, and FuWan Gan

***Abstract*—We propose and experimentally demonstrate the ultra-compact mode (de)multiplexers and polarization beam splitter (PBS) based on tapered bent asymmetric directional couplers. The strong coupling strength introduced by tapered bent waveguides significantly shortens the coupling length. As a result, high coupling and conversion efficiencies over a broad bandwidth can be obtained with small footprint. The coupling length of the fabricated PBS and mode (de)multiplexers are less than 4.9 μm and 8.7 μm, respectively. From 1534-1600 nm, the measured insertion loss (IL) is less than 1.4 and 1.55 dB for the TE_1-TE_0 and TE_2-TE_0 mode (de)multiplexers, respectively, and the crosstalk (CT) is less than -10 dB. The fabricated PBS shows low insertion loss of 0.55 dB and decent crosstalk of < -14 dB for both polarizations over an 85 nm wavelength range from 1505-1590 nm. Meanwhile, the larger fabrication tolerance ensures that the proposed devices can be readily fabricated with the standard complementary metal-oxide-semiconductor (CMOS) process.**

***Index Terms*—Silicon photonics, waveguide devices, polarization beam splitter, mode (de)multiplexer.**

I. Introduction

THE DEMAND of high-capacity data transmission and connectivity grows exponentially in the past decades [1]. Various on-chip integrated multiplexing technologies have been developed to increase the transmission scalability of a single fiber, including wavelength-division-multiplexing (WDM) [2], polarization-division-multiplexing (PDM) [3], mode-division-multiplexing (MDM) [4] and spatial-division-multiplexing (SDM) [5]. They can be realized by the photonic integrated circuits (PICs) built on the silicon-on-insulator (SOI) platform [6]. Coupled waveguide devices play an important role in such PICs for power splitting [7], polarization beam splitting [8] and rotation [9], mode multiplexing [10], etc. In these applications, light coupling between different modes is essential in the pursuit of following goals: low conversion/insertion loss, compactness, robustness against fabrication variations, and large bandwidth. Various approaches have been proposed and implemented to achieve those goals, such as structures based on directional couplers (DCs) [11], [12], sub-waveguide gratings (SWGs) [13], inverse design [14], asymmetric Y-branch [15], multimode interference (MMI) couplers [16] and adiabatic couplers (ACs) [17]. Among them, the ACs and MMI couplers can realize the goal of broadband and good fabrication tolerance. However, the sizes of the devices are usually large, which are not friendly for high-density silicon photonic integration. Asymmetric Y-branch can achieve large bandwidth and low crosstalk, but the mode conversion distance is relatively long. The inverse designed structures have attracted widespread concern recently, owing to their ultracompact size, while it is limited by the tight fabrication errors and small critical dimensions. The SWGs have relatively large footprint and the design and fabrication are also complex.

The DC-based structures are easy to design and fabricate, but the coupling length and coupling strength are required to be accurately controlled. Recently, there are more methods to improve the performance of the traditional DC-based structures, such as bent directional couplers [18], taper-etched directional couplers [19], tapered asymmetric directional couplers (TADCs) [20], and triple directional couplers (TDCs) [21], etc. In this work, we proposed and fabricated an ultracompact, low loss, broadband mode (de)multiplexer [(De)MUX] and polarization beam splitter (PBS), which have the advantage of TADCs and bent directional couplers. Compared with other DC-based structures, our devices are very compact, with coupling length less than 4.9 μm and 8.7 μm for PBS and mode (De)MUX, respectively. According to the analysis of fabrication tolerance, our devices are quite robust against fabrication variations. the measurement results show that the mode (De)MUX exhibits a

Manuscript received November 29, 2021; accepted December 13, 2021. Date of publication December 16, 2021; date of current version December 29, 2021. This work supported by in part by the National Key Research and Development Program of China under Grant 2017YFA0206403, in part by the Shanghai Municipal Science and Technology Major Project under Grant 2017SHZDZX03, in part by the Science and Technology Commission of Shanghai Municipality under Grant 16ZR1442600, and in part by the Strategic Priority Research Program of Chinese Academy of Sciences under Grant XDB24020400. *(Corresponding authors: Zhen Sheng; FuWan Gan.)*

JunBo Zhu, Yang Li, XiaoJuan She, Han Liao, Rui Huang, ZiJian Zhu, and Xiang Liu are with the State Key Laboratory of Functional Materials for Informatics, Shanghai Institute of Microsystem and Information Technology, Chinese Academy of Sciences, Shanghai 200050, China, and also with University of Chinese Academy of Sciences, Beijing 100049, China (e-mail: zjb@mail.sim.ac.cn; ylee@mail.sim.ac.cn; xiaojuanshe@mail.sim.ac.cn; liaohan@mail.sim.ac.cn; ruihuang@mail.sim.ac.cn; zhuzj@mail.sim.ac.cn; liuxiang@mail.sim.ac.cn).

HaiYang Huang, YingXuan Zhao, Zhen Sheng, and FuWan Gan are with the State Key Laboratory of Functional Materials for Informatics, Shanghai Institute of Microsystem and Information Technology, Chinese Academy of Sciences, Shanghai 200050, China (e-mail: huanghy@mail.sim.ac.cn; zhaoyx@mail.sim.ac.cn; zsheng@mail.sim.ac.cn; fuwan@mail.sim.ac.cn).

Digital Object Identifier 10.1109/JPHOT.2021.3135908

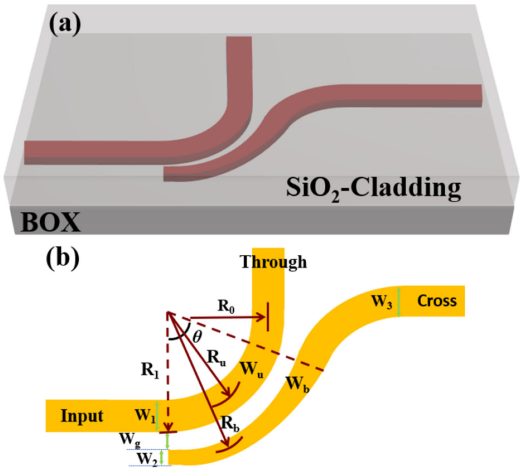

Fig. 1. Schematics of the proposed devices in (a) 3D view and (b) top view.

conversion loss of <1.55 dB and crosstalk of <−10 dB from 1.534 μm to 1.6 μm, and the PBS exhibits a low insertion loss of <0.55 dB and crosstalk of <−14 dB in the wavelength range from 1.505 μm to 1.59 μm.

II. Basic Operation Principles

As shown in Fig. 1, the devices are designed on SOI wafer with 220 nm thick top silicon layer, 2 μm thick buried oxide (BOX) and 2 μm thick upper SiO_2-Cladding. For bent waveguide, the Optical lengths (OPL) of different modes need to be calculated to satisfy the phase-matching condition, thus: $OPL = N_u \times R_u \times k_0 \times \theta = N_b \times R_b \times k_0 \times \theta$.

Where k_0 , θ are the wavenumber in the vacuum and the angle of the coupling region, respectively. N_u , R_u and N_b , R_b are the effective refractive indices and radii of the upper and bottom bent waveguides. The required equation can be simplified as follow: $N_u \times R_u = N_b \times R_b$.

R_1 is set to be 15 μm for both mode (De)MUX and PBS, which is large enough to achieve a low-loss for different modes and relatively compact size. The gap (W_g) between two waveguides is set to be 150 nm, in order to simplify the fabrication. For the upper waveguide, the width (W_u) remains unchanged, and the width (W_b) of the bottom waveguide gradually increases from W_2 to W_3. The radii of the upper and bottom waveguides are given by: $R_u = R_1 - W_u/2$ and $R_b = R_1 + W_g + W_b 2$, respectively.

Using the finite difference eigen mode (FDE) method, we calculated the relation between mode effective refractive indices and width of bent waveguide at wavelength of 1.55 μm. By using these parameters, the $N_{eff} \times R$ of the TE_0, TM_0, TE_1, TE_2 modes in the bent waveguides is calculated. For the mode (De)MUX and PBS, the introduced tapered bent structure of the bottom waveguide relaxes the phase matching condition, resulting in good robustness against variations in fabrication. Meanwhile, compared to the TE_0 mode, the weaker confinement of bent waveguide for TM_0, TE_1 and TE_2 make them easier to couple into the bottom waveguide, which results in stronger coupling strength between two waveguides. This is the reason why the proposed structures are much shorter than those DC-based structures.

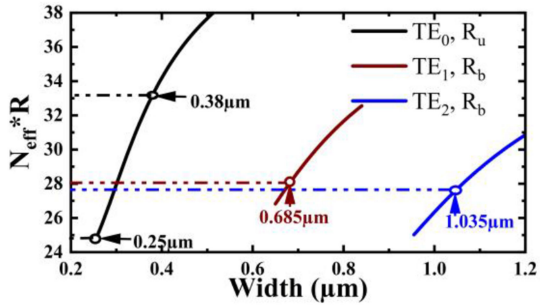

Fig. 2. Product of $N_{eff} \times R$ for the guided modes of the upper and bottom waveguides as a function of the waveguide width for the waveguide at the bending radii of $R_1 = 15$ μm.

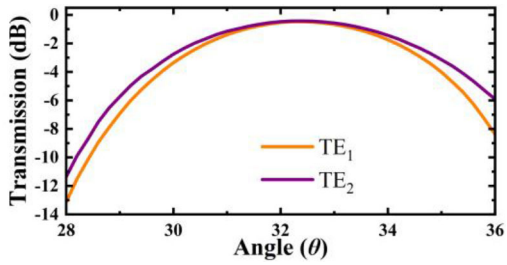

Fig. 3. Mode conversion loss for the TE_1-TE_0 and TE_2-TE_0, respectively.

TABLE I
The Device Parameters for Mode (De)MUXs

Type	W_1 (nm)	W_2 (nm)	W_3 (nm)	θ (degree)	R_0 (μm)
TE_1-TE_0	685	250	380	32.84	2.5
TE_2-TE_0	1035	250	380	32.76	5

III. Mode (De)Multiplexer

A. Structure and Design

To implement efficient mode conversion based on this structure, we use the following parameters: $W_2 = 250$ nm, $W_3 = 380$ nm and the W_u is determined with the relation of $N_{eff} \times R$ and waveguide width in Fig. 2. In order to satisfy the phase matching condition, the width of upper waveguide is chosen to be 0.684 μm and 1.035 μm for TE_1 and TE_2 modes, respectively. And the bend radius R_0 is chosen to be 2.5μm and 5 μm for the TE_1 and TE_2 mode (De)MUX, which helps filtering out the undesired high-order modes at through port and ensure low loss TE_0 mode propagation at the same time.

To complete the design, we need to calculate the angle (θ) of the coupling region, the coupling length (L_c) is denoted as $L_c = \theta\,(rad) \times R_1$. As shown in Fig. 3, we use 3D Finite-Difference Time-Domain (FDTD) method to sweep θ, and the value 32.84° and 32.76° show the best conversion efficiency for the TE_1-TE_0 and TE_2-TE_0, respectively.

Finally, the device parameters for mode (de)multiplexers are listed in Table I.

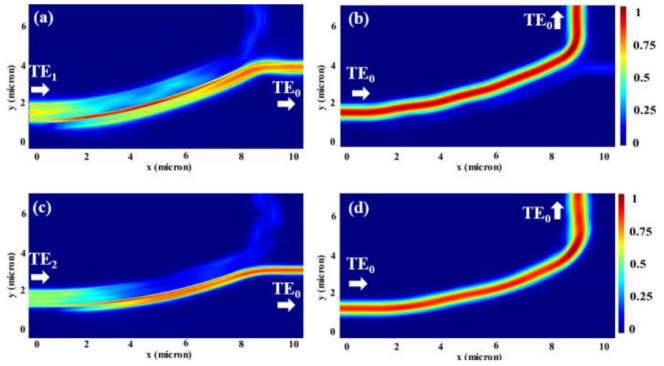

Fig. 4. Simulated mode propagation in the TE_1-TE_0 mode (de)multiplexer for the input (a) TE_1 mode and (b) TE_0 mode. And the TE_2-TE_0 mode (de)multiplexer for the input (c) TE_2 mode and (d) TE_0 mode.

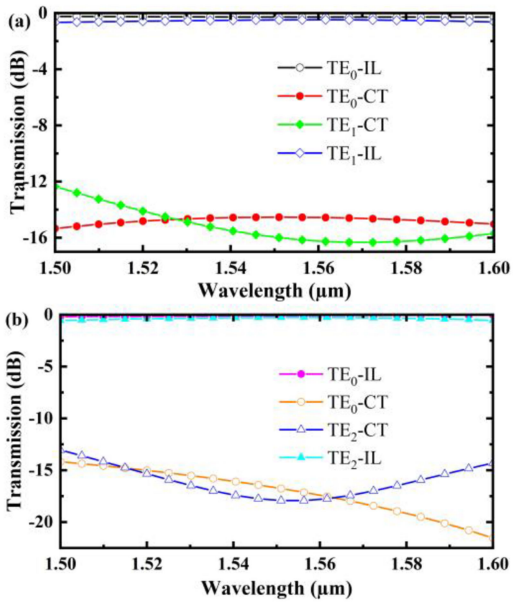

Fig. 5. Simulated transmission spectra of the (a) TE_1-TE_0 and (b) TE_2-TE_0 mode (de)multiplexer link over the wavelength range from 1.5 μm to 1.6 μm.

The simulated light propagation at the wavelength of 1.55 μm is shown in Fig. 4. High-order TE-polarized light is input, and coupled from the TE_1 and TE_2 modes in the upper bent waveguide into the TE_0 mode in the bottom bent waveguide, whereas the input TE_0 light can go directly along the through port with negligible losses. As we can see, the small bend can cause inter-mode crosstalk due to the asymmetric field distribution [22], thus we calculate the mode crosstalk introduced by mode conversion and tight waveguide bends, which we adopt the maximum crosstalk values from the output modes of in the through and cross ports in the transmission spectra.

As depicted in Fig. 5, in the case of TE_1-TE_0 mode (De)MUX, the insertion loss and the crosstalk are less than 0.65 dB and -12.4 dB from 1.5 μm to 1.6 μm for both input TE_1 and TE_0 modes. While in the case of TE_2-TE_0 mode (De)MUX, the IL and the CT are less than 0.55 dB and -13 dB for both input TE_2 and TE_0 modes in the wavelength range from 1.5 μm to 1.6 μm.

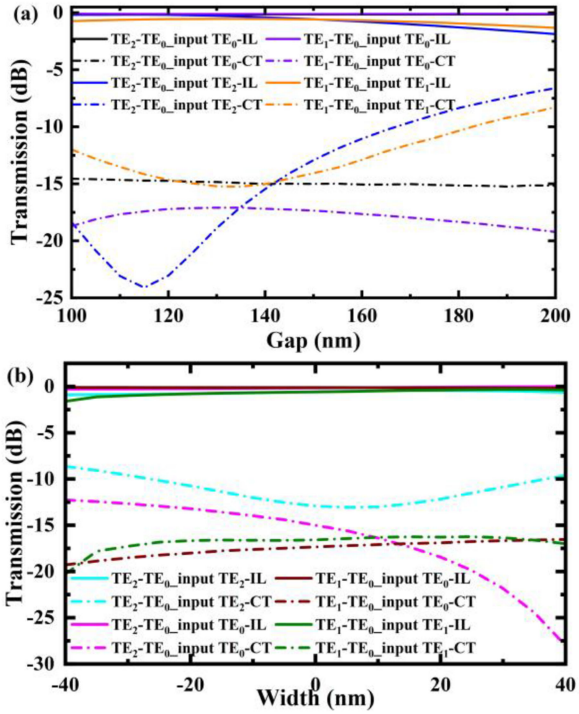

Fig. 6. Simulated fabrication tolerance to deviation of (a) the gap (W_g) and (b) the width (ΔW) for the mode (de)multiplexers.

Furthermore, we analyzed the fabrication tolerance of the proposed mode (De)MUX using 3D-FDTD method by changing the waveguide width and the gap (W_g). The performance of mode (De)MUX is more sensitive to the width of unchanged waveguide, so the width variation (ΔW) of upper waveguide W_u is changed to investigate the fabrication tolerance. Fig. 6 show the calculated IL and CT as a function of ΔW and the gap Wg. As the gap Wg varies from 100 to 167 nm, the IL and CT are below 1 dB and -10 dB for the TE_1-TE_0 and TE_2-TE_0 mode (De)MUX. And the IL and CT are less than 1 dB and -10 dB within the waveguide width variation ΔW of $+40$ nm$\sim$-23 nm, $+35$ nm$\sim$-25 nm for TE_1-TE_0 and TE_2-TE_0, respectively. The asymmetric directional coupler suggested only 5 nm fabrication error is acceptable [23], and for the optimized taper asymmetric directional coupler, the IL can remain less than 1.8 dB with the fabrication error in range $\pm$10 nm [24].

B. Fabrication and Measurement

The fabrication procedures of the devices are as follow. First, electron-beam lithography (EBL) was applied to define the patterns of devices, then the patterns were transferred onto the silicon layer by inductively coupled plasma (ICP) dry-etching. Finally, a 2-μm-thick SiO_2 upper cladding was deposited on the devices with plasma enhanced chemical vapor deposition (PEVDC) process. The microscope images of the fabricated mode (De)MUX links are shown in Fig. 7, and a pair of reference grating coupler is also fabricated on the same chip to normalize the spectral responses.

In the measurements, the light from a tunable laser (Keysight 81600B) was adjusted by a polarization controller (PC) and

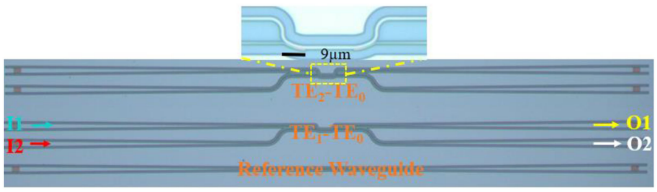

Fig. 7. Microscope photos of the fabricated mode (De)MUX links.

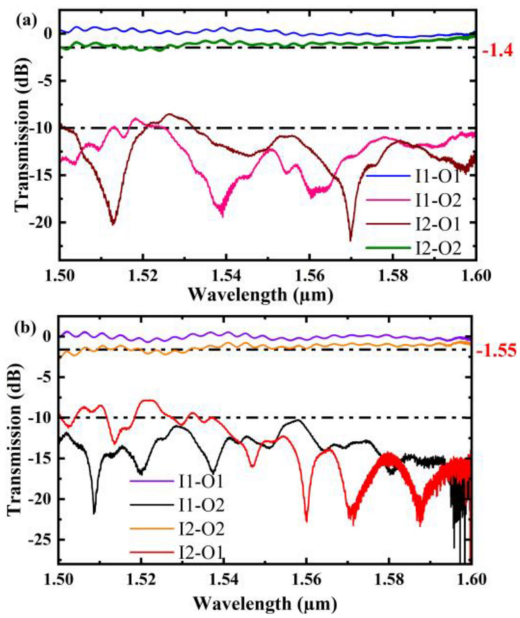

Fig. 8. Measured transmission spectra of the fabricated (a) TE_1-TE_0 and (b) TE_2-TE_0 (De)MUX link.

coupled into and out of the chip by fibers. The output light was collected by a power meter and a photodetector to characterize the transmission performance. Fig. 8(a) shows the measured transmission spectra of the mode (De)MUX link of TE_1-TE_0. When the TE_0 mode is launched at the port I1, the mode IL and CT are lower than 0.5 dB and -10 dB from 1.525 μm to 1.6 μm. When the TE_0 mode is launched at the port I2, the mode IL and CT are lower than 1.4 dB and -10 dB over the wavelength ranging from 1.533 μm to 1.6 μm. The measurement results of TE_2-TE_0 mode (De)MUX link are shown in Fig. 8(b), for the TE_0 mode launched from I1 and I2 separately, the mode IL and CT are less than 1.55 dB and -10 dB in the wavelength range from 1.534 μm to 1.6 μm. The deviation of loss from the simulated value may result from the imperfection introduced during the fabrication.

Table II compares the reported experimental mode (de)multiplexers, the devices we proposed exhibit a very compact footprint with high performance. Optimal Euler curves [25] or Bezier curves [26] can be adopted to improve the inter-mode crosstalk due to the mode mismatch at the interface when the multimode straight and bent waveguides and bent waveguides with different radius are interconnected. Meanwhile, using cascaded tapered bent ADCs, the crosstalk can also be further reduced.

TABLE II
COMPARISON OF THE REPORTED FABRICATED SILICON MODE (DE)MULTIPLEXERS

Ref / Year	Type	IL (dB)	CT (dB)	Coupling length (μm)	Bandwidth (nm)
[21] / 2021	TE_1-TE_0	2.3	< -14	48	1500 - 1600
[27] / 2018	TE_1-TE_0	0.56 (1550nm)	< -9.1	60	1513 - 1619
[28] / 2017	TE_1-TE_0 TE_2-TE_0	1.1	< -24	150	1513 - 1619
[29] / 2020	TE_1-TE_0 TE_2-TE_0	1.5 0.5	< -6 < -8	7.66	1525 - 1565
[30] / 2020	TE_1-TE_0	2	< -8	2.42	1520 - 1580
this work	TE_1-TE_0 TE_2-TE_0	1.4 1.55	< -10	~ 8.7	1534 - 1600

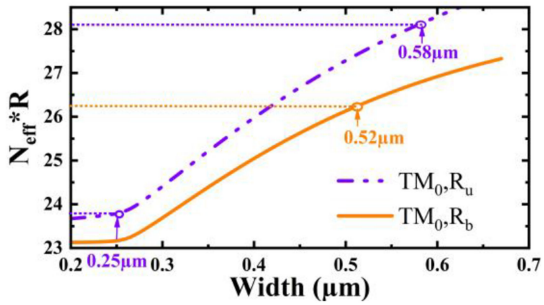

Fig. 9. Product of $N_{eff} \times R$ for the TM_0 mode of the upper and bottom waveguides as a function of the waveguide width for the waveguide at the bending radii of $R_1 = 15$ μm.

IV. POLARIZATION BEAM SPLITTER

A. Structure and Design

The proposed structure can also be used to realize polarization beam splitting. The width of bottom waveguide increases from $W_2 = 250$ nm to $W_3 = 580$ nm, and according to the phase matching condition, the width (W_u) of upper waveguide is chosen to be 520 nm, shown in Fig. 9. It is well known that TM_0 mode has a higher bending loss than TE_0 mode, then the radius (R_0) of 2 μm is adopted at the through port to filter out the residual TM-polarized light. As the design procedure of mode (De)MUX, the value of coupling angle (θ) is chosen to be 17.6° which exhibits the best insertion loss for both TE_0 and TM_0 modes.

Fig. 10(a) and (b) show the light propagation for input TM_0 and TE_0 mode, respectively. When the TM_0 mode is launched in the upper waveguide, the light is coupled and output from the cross port, while the input TE_0 mode is output from the through port. Fig. 10(c) show the simulated IL and CT when the input is TE_0 and TM_0 mode, respectively. The IL and CT are lower than 0.46 dB and -12 dB in the wavelength ranging from 1.5 to 1.6 μm.

The fabrication tolerance of the PBS is also investigated. As shown in Fig. 11, we simulated the impact of the waveguide width variation ΔW and the gap W_g on the CT and IL of the designed PBS at 1.55 μm. Within the waveguide width variation

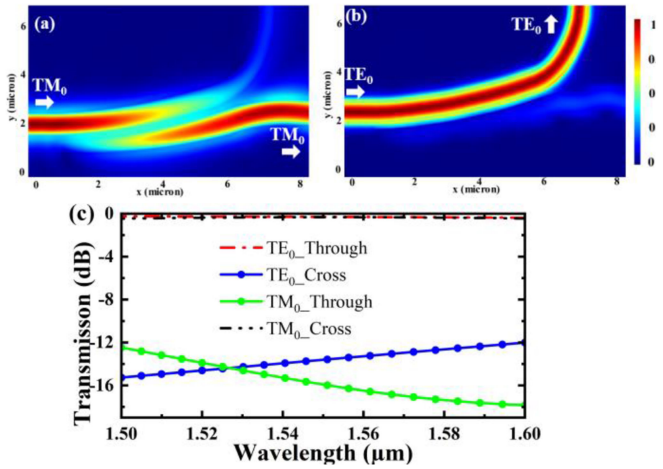

Fig. 10. Simulated mode propagation in the PBS for the input (a) TM_0 mode and (b) TE_0 mode, and the (c) transmission spectra of the PBS.

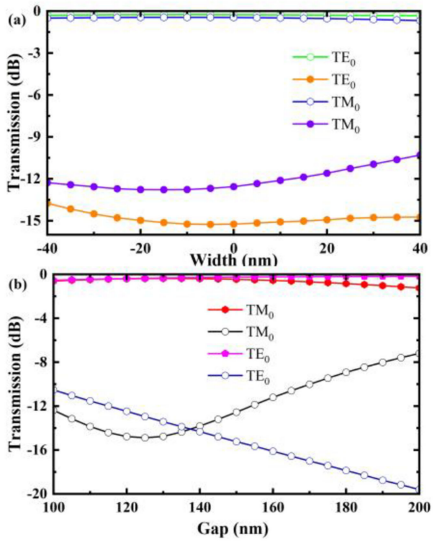

Fig. 11. Simulated fabrication tolerance to deviation of (a) the width (ΔW) and (b) the gap (W_g) for the PBS.

ΔW of $\pm$ 40 nm, the results show that the IL and CT are less than 0.33 dB and -13.7 dB for input TE_0 mode, while the IL and CT are less than 0.68 dB and -10 dB for the input TM_0 mode. When the gap W_g varies from 100 to 170 nm, the IL and CT are lower than 0.7 dB and -10 dB for the input TE_0 and TM_0 modes.

B. Fabrication and Measurement

Following the same fabrication procedures of mode (De)MUX links, we also fabricated the designed PBS on SOI wafer. Fig. 12 displays the microscope and scanning electron microscopic (SEM) images of the fabricated PBSs together with test structures. Two identical PBSs connected with TE- and TM-type grating couplers (GCs) are fabricated, respectively, which are to characterize the transmission spectra of input TE- and TM-polarized light. The reference straight waveguides with TE-type and TM-type grating couplers are also fabricated, respectively, to normalize the transmission spectra.

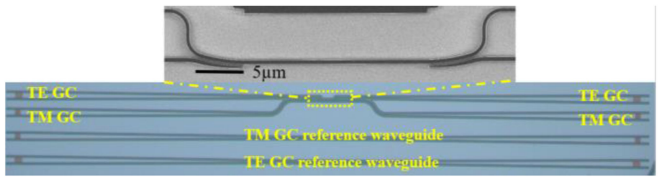

Fig. 12. Microscope and SEM photos of the fabricated devices.

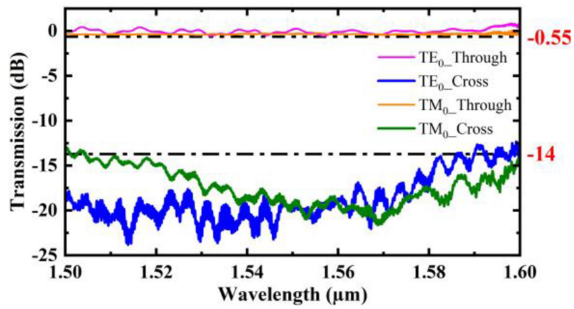

Fig. 13. Measured transmission spectra of the fabricated PBS.

TABLE III
COMPARISON OF THE REPORTED FABRICATED PBSS ON SOI PLATFORM

Ref / Year	IL (dB)	CT (dB)	Coupling length (μm)	Bandwidth (nm)
[31] / 2017	2	< -30	26	1520 - 1610
[32] / 2019	2	< -20	71.5	1522 - 1599
[33] / 2019	5	< -10	7	1535 - 1565
[34] / 2021	1.53	< -14.22	6	1527 - 1580
[35] / 2019	1.39	< -11.98	26.44	1510 - 1590
this work	0.55	< -14	~ 4.9	1509 - 1590

The measured transmission spectra in TE- and TM- polarizations are shown in Fig. 13. The measured IL and CT are below 0.55 dB and -14 dB from 1.505 to 1.59 μm for the input TE- and TM- polarizations. Table III lists the comparison of our device with some reported PBSs fabricated on SOI wafer. Our PBS performs an ultra-compact coupling length, low-loss within broad bandwidth range. The polarization crosstalk can be further improved with cascaded structures [11].

V. CONCLUSION

In conclusion, we have proposed and demonstrated the ultra-compact, high-performance silicon mode (de)multiplexers and PBS employing tapered bent asymmetric directional coupler. The structure of tapered bent asymmetric directional coupler significantly reduces the coupling length, which are less than 8.7 μm and 4.9 μm for the introduced silicon mode (De)MUX and PBS. Also, the fabrication tolerance analysis exhibits great robustness against the variations of the width and gap. Our experimental results reveal that, in the wavelength range of 1534-1600 nm, the IL are less than 1.4 and 1.55 dB for the

TE_1-TE_0 and TE_2-TE_0 mode (De)MUX, respectively, and the crosstalk is less than -10 dB. The fabricated PBS has a low loss of 0.55 dB and decent crosstalk of $<$-14 dB for both polarizations from 1505-1590 nm. In further work, the crosstalk of the mode (De)MUX and PBS can be further improved with cascaded structures [11] and optimal curves [25], [26], etc. Moreover, this mode (De)MUX can be readily extended to higher order mode (De)MUX. Owing to excellent CMOS compatibility, good scalability, low insertion loss, compact footprint, and broad bandwidth, we believe that the proposed devices can be potentially integrated with other multiplexing schemes to further increase the transmission capacity in high-density optical network.

REFERENCES

[1] A. H. Atabaki *et al.*, "Integrating photonics with silicon nanoelectronics for the next generation of systems on a chip," *Nature*, vol. 556, no. 7701, pp. 349–354, 2018.

[2] Y. Tan, H. Wu, and D. X. Dai, "Silicon-based hybrid (de)Multiplexer for wavelength-/polarization-division-multiplexing," *J. Lightw. Technol.*, vol. 36, no. 11, pp. 2051–2058, Jun. 2018.

[3] S. T. Chen, Y. C. Shi, S. L. He, and D. X. Dai, "Compact monolithically-integrated hybrid (de)multiplexer based on silicon-on-insulator nanowires for PDM-WDM systems," *Opt. Exp.*, vol. 23, no. 10, pp. 12840–12849, 2015.

[4] D. X. Dai and J. E. Bowers, "Silicon-based on-chip multiplexing technologies and devices for Peta-bit optical interconnects," *Nanophotonics*, vol. 3, pp. 283–311, 2014.

[5] D. J. Richardson, J. M. Fini, and L. E. Nelson, "Space-division multiplexing in optical fibres," *Nature Photon.*, vol. 4, no. 5, pp. 354–362, 2013.

[6] R. Kirchain and L. Kimerling, "A roadmap for nanophotonics," *Nature Photon.*, vol. 1, no. 6, pp. 303–305, 2007.

[7] K. Xu *et al.*, "Integrated photonic power divider with arbitrary power ratios," *Opt. Lett.*, vol. 42, pp. 855–858, 2017.

[8] S. Mao, L. Cheng, C. Zhao, and H. Y. Fu, "Ultra-broadband and ultra-compact polarization beam splitter based on a tapered subwavelength-grating waveguide and slot waveguide," *Opt. Exp.*, vol. 29, no. 18, 2021, Art. no. 28066.

[9] L. Liu, Y. H. Ding, K. Yvind, and J. M. Hvam, "Silicon-on-insulator polarization splitting and rotating device for polarization diversity circuits," *Opt. Exp.*, vol. 19, no. 13, pp. 12646–12651, 2011.

[10] D. X. Dai *et al.*, "10-Channel Mode (de)multiplexer with dual polarizations," *Laser Photon. Rev.*, vol. 12, no. 1, pp. 9, 2018.

[11] H. Wu, Y. Tan, and D. X. Dai, "Ultra-broadband high-performance polarizing beam splitter on silicon," *Opt. Exp.*, vol. 25, no. 6, pp. 6069–6079, 2017.

[12] F. Zhang, H. Yun, Y. Wang, Z. Lu, L. Chrostowski, and N. A. F. Jaeger, "Compact broadband polarization beam splitter using a symmetric directional coupler with sinusoidal bends," *Opt. Lett.*, vol. 42, no. 2, pp. 235–238, 2017.

[13] L. Sun, R. Hu, Z. H. Zhang, Y. He, and Y. K. Su, "Ultrabroadband power coupling and mode-order conversion based on trapezoidal subwavelength gratings," *IEEE J. Sel. Top. Quantum Electron.*, vol. 27, no. 6, Nov./Dec. 2021, Art. no. 8100308.

[14] Y. J. Liu *et al.*, "Arbitrarily routed mode-division multiplexed photonic circuits for dense integration," *Nat. Commun.*, vol. 10, pp. 1–7, 2019.

[15] W. W. Chen *et al.*, "Silicon three-mode (de)multiplexer based on cascaded asymmetric y junctions," *Opt. Lett.*, vol. 41, no. 12, pp. 2851–2854, 2016.

[16] X. Sun, J. S. Aitchison, and M. Mojahedi, "Realization of an ultra-compact polarization beam splitter using asymmetric MMI based on silicon nitride /silicon-on-insulator platform," *Opt. Exp.*, vol. 25, no. 7, pp. 8296–8305, 2017.

[17] J. Wang *et al.*, "Broadband and fabrication-tolerant on-chip scalable mode-division multiplexing based on mode-evolution counter-tapered couplers," *Opt. Lett.*, vol. 40, no. 9, pp. 1956–1959, 2015.

[18] J. Wang, D. Liang, Y. B. Tang, D. X. Dai, and J. E. Bowers, "Realization of an ultra-short silicon polarization beam splitter with an asymmetrical bent directional coupler," *Opt. Lett.*, vol. 38, no. 1, pp. 4–6, 2013.

[19] Y. Sun, Y. L. Xiong, and W. N. Ye, "Experimental demonstration of a two-mode (de)multiplexer based on a taper-etched directional coupler," *Opt. Lett.*, vol. 41, no. 16, pp. 3743–3746, 2016.

[20] H. Shu, B. Shen, Q. Deng, M. Jin, X. Wang, and Z. Zhou, "A design guideline for mode (DE) multiplexer based on integrated tapered asymmetric directional coupler," *IEEE Photon. J.*, vol. 11, no. 5, Oct. 2019, Art. no. 6603112.

[21] W. Jiang, S. Xu, and H. Zhang, "Broadband mode (De)Multiplexer formed with phase-matching of multimode access-waveguide," *IEEE Photon. Technol. Lett.*, vol. 33, no. 8, pp. 415–418, Apr. 2021.

[22] X. Jiang, H. Wu, and D. Dai, "Low-loss and low-crosstalk multimode waveguide bend on silicon," *Opt. Exp.*, vol. 26, no. 13, pp. 17680–17689, 2018.

[23] C. Pan and B. A. Rahman, "Accurate analysis of the mode (de)multiplexer using asymmetric directional coupler," *J. Lightw. Technol.*, vol. 34, no. 9, pp. 2288–2296, May 2016.

[24] B. Shen, H. Shu, L. Zhou, and X. Wang, "A design method for high fabrication tolerance integrated optical mode multiplexer," *Sci. China (Inf. Sci.)*, vol. 63, no. 6, pp. 184–194, 2020.

[25] D. Yi, Y. Zhang, and H. K. Tsang, "Optimal Bezier curve transition for low-loss ultra-compact S-bends," *Opt. Lett.*, vol. 46, no. 4, pp. 876–879, 2021.

[26] X. R. Wu *et al.*, "Low crosstalk bent multimode waveguide for on-chip mode-division multiplexing interconnects," in *Proc. Conf. Lasers Electro-Opt.*, 2018, paper JW2A.66.

[27] H. Q. Li *et al.*, "Experimental demonstration of a broadband two-mode multi/demultiplexer based on asymmetric Y-junctions," *Opt. Laser Technol.*, vol. 100, pp. 7–11, 2018.

[28] D. Guo and T. Chu, "Silicon mode (de)multiplexers with parameters optimized using shortcuts to adiabaticity," *Opt. Exp.*, vol. 25, no. 8, pp. 9160–9170, 2017.

[29] L. J. Hao *et al.*, "Experimental demonstration of compact mode converter based on conformal dielectric metasurface," *IEEE Photon. Technol. Lett.*, vol. 32, no. 18, pp. 1143–1146, Sep. 2020.

[30] C. N. Yao *et al.*, "Dielectric nanoaperture metasurfaces in silicon waveguides for efficient and broadband mode conversion with an ultrasmall footprint," *Adv. Opt. Mater.*, vol. 8, no. 17, pp. 8, 2020.

[31] J. R. Ong *et al.*, "Broadband silicon polarization beam splitter with a high extinction ratio using a triple-bent-waveguide directional coupler," *Opt. Lett.*, vol. 42, no. 21, pp. 4450–4453, 2017.

[32] L. Xu *et al.*, "Compact broadband polarization beam splitter based on multimode interference coupler with internal photonic crystal for the SOI platform," *J. Lightw. Technol.*, vol. 37, no. 4, pp. 1231–1240, Feb. 2019.

[33] Z. Cheng, J. Wang, Y. Q. Huang, and X. M. Ren, "Realization of a compact broadband polarization beam splitter using the three-waveguide coupler," *IEEE Photon. Technol. Lett.*, vol. 31, no. 22, pp. 1807–1810, Nov. 2019.

[34] Y. Liu *et al.*, "Direct-binary-search-optimized compact silicon-based polarization beam splitter using a pixelated directional coupler," *Opt. Commun.*, vol. 484, 2021, Art. no. 126670.

[35] N. Zhao, C. Y. Qiu, Y. He, Y. Zhang, and Y. K. Su, "Broadband polarization beam splitter by using cascaded tapered bent directional couplers," *IEEE Photon. J.*, vol. 11, no. 4, Aug. 2019, Art. no. 4900808.